Effects on the crystallization behavior and biocompatibility of poly(LLA-ran-PDO-ran-GA) with poly(D-lactide) as nucleating agents

Tiantang Fan, ![ID] †*[a] Jingwen Qin,†[b] Fen Dong,†[d] Xiao Meng,[e] Yanqi Li,[a] Ying Wang,[a] Qing Liu*[bc] and Guannan Wang ![ID] *[a]

The blends of poly(L-lactide acid-*p*-dioxanone-glycolide) (PLPG) with poly(D-lactide) (PDLA) (PLPG/PDLA) were prepared by a solution-casting method. The effects of PDLA on the properties of the PLPG were studied. DSC and WAXD results confirmed that PLA stereocomplex (sc-PLA) crystals were formed by blending PLLA segments in PLPG with PDLA, and the melting endotherm for both PLLA and sc-PLA relied on PDLA content. The non-isothermal crystallization results indicated that the crystallization process was remarkably accelerated by the addition of PDLA. Meanwhile, the results of isothermal crystallization indicated that the half-time of crystallization decreased with the increase of PDLA content. Besides, the enzymatic degradation behavior of the samples showed that with the increase of PDLA content, the mass loss gradually decreased. Furthermore, TGA and DTG results indicated that the thermal degradation of the samples was a complex process. Moreover, the biocompatibility of the samples was tested by cell culture and using CCK-8 and live/dead staining. Results showed that the samples possessed lower cytotoxicity. Therefore, the PLPG/PDLA blends are promising candidate materials in biomedical applications.

Introduction

As a biomaterial, poly(L-lactide) (PLLA) has received much attention due to its excellent biocompatibility, biodegradability and processability. It has been widely used in drug release systems, tissues engineering, cardiovascular implants such as biodegradable stents and so on.[1–4] Nevertheless, PLLA has certain issues such as brittleness and degradation rate,[5,6] which limit its biomedical applications. Hence, considerable research has been carried out by blending or copolymerization with flexible polymers trying to overcome these issues. Specifically, copolymerization with flexible polymer segments has been known as the effective method to regulate the properties of PLLA. Poly(*p*-dioxanone) (PPDO) has been widely used in fabrication of surgical sutures, drug delivery systems, bone tissue fixation devices and other biomedical products due to its

excellent flexibility and high retention rate of mechanical strength during degradation.[7–9] Meanwhile, poly(L-lactide-*co*-glycolide) (PLGA) has been widely used as a biomaterial due to its good mechanical properties and degradation behavior.[10–13] Here, in view of the shortcomings of PLLA, a new PLLA–PDO–GA (PLPG) terpolymer was synthesized by ring-opening polymerization aimed for biomedical applications. However, the PLPG terpolymer has good degradation rate and toughness, but the addition of PDO and GA would decrease the crystallization ability of PLLA. Hence, it is necessary to study the crystallization mechanism of the PLPG terpolymers so as to enhance its crystallization capacity.

Crystallization ability of PLLA copolymers can be enhanced by nucleating agents.[14–16] For example, inorganic nucleating agents, including graphene oxide (GO), cellulose nanocrystals and montmorillonite (MMT), were used to accelerate the crystallization ability of PLLA copolymers.[17–23] Zhao *et al.*[17] showed that PLLA could complete the crystallization with the introduction of 2.5 wt% MMT, and the crystallization half-time ($t_{1/2}$) decreased significantly. Samira *et al.*[24] pointed out that the crystallization kinetics of PLLA in the presence of GO and PEG-*g*-GO, and the isothermal crystallization results showed reduction of nucleation due to clustering of nanoparticles at higher contents of GO and GO-*g*-PEG (1.5 wt%), leading to a higher overall rate of crystallization. However, not all inorganic nucleating agents are suitable for biomedical applications because of their easy migration and non-degradation nature. Wan *et al.*[25] showed that using PDLA (≤1% w/

[a]College of Medical Engineering & the Key Laboratory for Medical Functional Nanomaterials, Jining Medical University, Jining, 272067, P. R. China. E-mail: chemwangguannan@gmail.com; 17110300011@fudan.edu.cn

[b]The Institute for Translational Nanomedicine, Shanghai East Hospital, The Institute for Biomedical Engineering & Nano Science, Tongji University School of Medicine, Shanghai 200092, P. R. China. E-mail: qliu@ametcorp.com

[c]Beijing Advanced Medical Technologies, Ltd Inc., Beijing 100085, People's Republic of China

[d]Affiliated Hospital of Jianghan University, Wuhan City, 430015, P. R. China

[e]Nanjing Recongene Biomedical Technologies, Ltd Inc., Nanjing, 210032, P. R. China

† These three authors are contributed equally to this work.

w) would manipulate the morphology and crystallization of PLLA/PCL blends.

Up to now, there has been increasing attention to the crystallization behavior of asymmetric blends including both homopolymer and stereocomplexes. Therefore, stereocomplex of poly(lactic acid) (sc-PLA) formed by the hydrogen bond interaction between poly(L-lactide) (PLLA) and poly(D-lactide) (PDLA) has been regarded as one of the most promising methods to accelerate the crystallinity ability of PLLA copolymers.[26–28] The melting temperature (T_m) of sc-PLA is around 230 °C, which is 50 °C higher than that of PLLA or PDLA.[29–31] Hence, sc-PLA could be retained in PLLA under melt condition. Moreover, because of the extremely high radius growth rate, the overall crystallization rate of sc-PLA is higher. Sc-PLA crystals have been used as the nucleating agents to offer heterogeneous nucleation sites for PLLA crystallization.[32] It is reported that sc-PLA crystals can be formed *in situ* even if a small amount of PDLA was added into PLLA matrix, and the crystallization ability of PLLA is significantly increased. And the introduction of a small amount of PDLA could strengthen the nucleation process of PLLA significantly and thus enhance the overall crystallization rate of PLLA. On the other hand, the introduction of PDLA could generate sc-PLA *in situ* in PLPG matrix, which reduces interfacial tension and improves interphase adhesion. Su *et al.*[33] reported that the sc-PLA was successfully prepared by PDLA and PLLA using a melt-blending method, and the degree of crystallinity of the sc-PLA reached 43.7%. The tensile strength, elastic modulus, elongation at break and fracture work of sc-PLA were 83.70 MPa, 2.04 GPa, 5.16%, and 258 kJ m^{-3}, respectively. Fan *et al.*[27] reported that PDLA significantly enhanced the crystallization kinetics of PLLA segments in the PTLG/PDLA blends, and $t_{0.5}$ decreased from 14.4 to 6.0 minutes at 100 °C as the content of PDLA increased from 3 wt% to 20 wt%. Hence, the stereocomplextion of PLLA and PDLA is regarded as an effective way to enhance the crystallization properties of PLLA copolymers.

The aim of this paper is to enhance the crystallization ability of PLLA segments in PLPG by adding PDLA. The crystallization behavior of PLPG terpolymers and the influence of the PDLA on the crystalline properties of the PLPG/PDLA blends were studied.

Experimental

Materials

L-Lactide (L-LA), D-lactide (D-LA) and glycolic acid (GA) were purchased from Daigang Biomaterial (China). P-Dioxanone (PDO) and tannous octoate (Sn(Oct)$_2$) were obtained from Bangcheng Chems (Shanghai, China) and Adamas Reagent Co. Ltd (Shanghai, China), respectively. All chemicals and materials were used as received unless otherwise noted.

Preparation of the samples

PLPG terpolymers were synthesized by ring-opening polymerization (ROP) of LLA, PDO and GA with Sn(Oct)$_2$ as catalyst. Number-average molecular weight ($\bar{M}_n$) of PLPG was 6.4×10^5 g mol^{-1}. And Scheme 1 illustrates the synthesis route and structure of PLPG terpolymers.

PLPG/PDLA blends were obtained by solution-casting method at room temperature. Briefly, PLPG and PDLA were dissolved in CH$_2$Cl$_2$ for 3 h under stirring. Then, CH$_2$Cl$_2$ was evaporated at room temperature for 24 h. Finally, PLPG/PDLA blends were put in a vacuum drying oven (45 °C) for 48 h. The weight ratios of PDLA in the samples were set as 5, 10, 15 and 20 wt%. For instance, PLPG/PDLA-5 represents PLPG/PDLA blends with 5 wt% of PDLA.

Characterizations

Wide Angle X-ray Diffraction (WAXD) was performed on a Bruker D8 Advance X-ray diffractometer to study the crystal structure of the samples ($\lambda = 0.154$ nm, 40 kV, 40 mA). The scanning 2θ was obtained from 5° to 35° with a scanning speed of 4° min^{-1}.

The thermal behavior of the samples was analyzed by DSC (Mettler Toledo, DSC1/700, Switzerland) under nitrogen atmosphere. In particular, the samples were heated to 230 °C at 20 °C min^{-1} and maintained for 3 min to remove history. Then, the samples were quenched to room temperature. Finally, the samples were heated to 230 °C at a speed of 10 °C min^{-1}. The degree of crystallinity of PLLA ($X_{c\text{-hc}}$) and sc-PLA crystals ($X_{c\text{-sc}}$) were obtained from the second heating scanning. $X_{c\text{-hc}}$ and $X_{c\text{-sc}}$ were calculated by the follow eqn (1) and (2), respectively.

$$X_{c\text{-hc}} = \Delta H_{m\text{-hc}}/\Delta H_{m\text{-hc}}^{\infty} \quad (1)$$

$$X_{c\text{-sc}} = \Delta H_{m\text{-sc}}/\Delta H_{m\text{-sc}}^{\infty} \quad (2)$$

where $\Delta H_{m\text{-hc}}$ and $\Delta H_{m\text{-sc}}$ were the melting enthalpy of PLLA and sc-PLA crystals, respectively. ΔH_m^{∞} is the theoretical value of melting enthalpy for 100% crystallized PLLA and sc-PLA that is 94 J g^{-1} and 150 J g^{-1}, respectively.[34,35] The total crystallinity of the samples was calculated by the follow eqn (3):

$$X_{c\text{-hc+sc}} = X_{c\text{-hc}} + X_{c\text{-sc}} \quad (3)$$

For non-isothermal crystallization and isothermal crystallization behavior, the samples of 5–10 mg were heated at

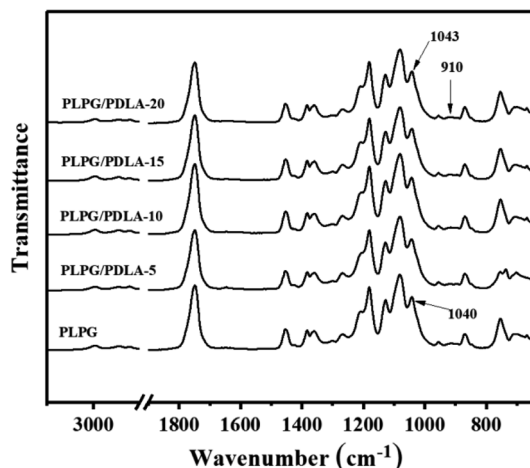**Scheme 1** Synthesis route and structure formula of the PLPG terpolymers.

© 2022 The Author(s). Published by the Royal Society of Chemistry

Fig. 1   FTIR of the samples.

$$W(\%) = \frac{(M_i - M_d)}{M_i} \times 100 \qquad (4)$$

where M_i and M_d were the initial weight and final weight of the samples, respectively.

Thermal degradation

Thermogravimetric analysis (Hengjiu, Beijing) was performed to examine the thermal degradation kinetics of the blends and PLPG matrix. Briefly, the samples were heated to 450 °C at rate of 10, 15, 20 and 25 °C min^{-1}, respectively.

Cytotoxicity assay

Human adipose derived stem cells (hADSCs) were used to study the cytotoxicity of the samples. The viability of the cells was analyzed by the live/dead staining assay. In brief, hADSCs suspension (6×10^4 cells per mL) were cultured in 96-well plates containing the 2 mL extracts of the samples. After cultured for 24, 48 and 72 h in an incubator (5% CO_2, 37 °C), the hADSCs were stained using calcein-AM (2 μM) and propidium iodide (8 μM) solution for 30 minutes. Then, the hADSCs were rinsed with PBS for 3 times. Finally, the viability of hADSCs was evaluated under a fluorescence microscope. Three parallel samples were used for each experiment.

Cell proliferation assay

The proliferation of hADSCs cultured in extracts of the samples was quantitatively studied by the CCK-8 assays. In brief, 6×10^4 cells per mL hADSCs were transferred into 96-well plates that contained the extracts of the samples, and then put into an incubator at 37 °C with 5% CO_2. When cultured for 24, 48 and 72 h, 10 μL of CCK-8 solution (100 μL, 10%) was put into each well in the dark and incubated for 2 h. The absorbance was recorded by Multimode Reader (Infinite M200PRO, Tecan, Switzerland) at 450 nm. Three parallel samples were used for each experiment.
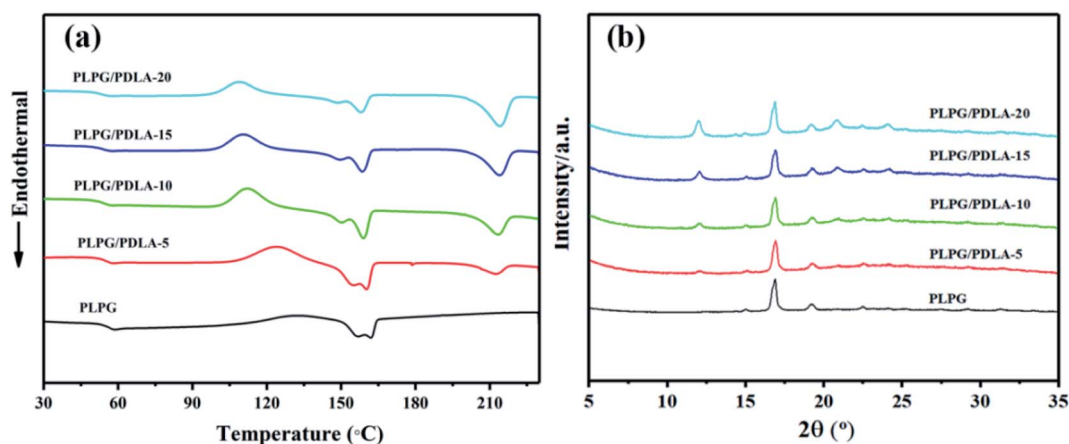
50 °C min^{-1} to 230 °C and kept for 5 min. Then, the samples were cooled to room temperature at 2.5 °C min^{-1}. To study the crystallization accelerating effect of the formed sc-PLA crystals in the samples, the samples were heated up to 230 °C and held for 3 min, and then quenched to the selected isothermal crystallization temperature (T_c) of 100, 105, 110 and 115 °C.

Enzymatic degradation

Enzymatic degradation of the samples was studied by proteinase K for 14 days. Briefly, the samples were cut into square specimens ($5 \times 5 \times 0.1$ mm) and specimens weight was measured in triplicates before and after soaking in 2 mL proteinase K–tris buffer solution (0.05 M, pH = 8.5). The solution was renewed every 3 days to maintain the activity of proteinase K. Then, the samples were taken out at the particular immersion time, washed with distilled water for 3 times. Finally, the samples were dried at 37 °C for several days until the weight of the samples was constant. The mass loss (W) of the sample was calculated using the eqn (4):

Fig. 2   DSC second melting curves at 10 °C min^{-1} (a) and WAXD of the samples (b).

Table 1 Thermal properties of the samples in DSC second melting curves

Samples	T_g (°C)	T_{m1} (°C)	$\Delta H_{m\text{-}hc}$ (J g^{-1})	$X_{c\text{-}hc}$ (%)	T_{m2} (°C)	$\Delta H_{m\text{-}sc}$ (J g^{-1})	$X_{c\text{-}sc}$ (%)	$X_{c\text{-}hc+sc}$ (%)
PLPG	54.26	161.87	28.33	29.82	—	—	—	—
PLPG/PDLA-5	54.38	160.49	27.30	29.35	212.36	7.57	4.88	32.18
PLPG/PDLA-10	54.26	159.07	22.61	24.31	213.32	15.18	9.79	34.10
PLPG/PDLA-15	53.30	158.61	19.99	21.49	213.78	20.85	13.45	34.94
PLPG/PDLA-20	52.74	157.89	16.75	18.01	213.99	26.19	16.90	34.91

Immunofluorescent staining

The hADSCs, after being cultured in extracts of the samples, were fixed with paraformaldehyde (4%) for 15 min, and then washed 3 times with PBS. The hADSCs were permeabilized with Triton X-100 solution (0.5%) for 10 min. The actin stress fibers of hADSCs were stained by the RBITC-labeled phalloidin solution (1 : 200 dilution) for 30 min in the dark. Then, DAPI (5 μg mL^{-1}) was used to stain the cell nuclear. After staining, cells were observed under a fluorescence microscope and fluorescent pictures were captured.

Results and discussion

Structure of the samples

Fig. 1 showed the FTIR spectra of the samples. As seen, compared with PLPG matrix, the PLPG/PDLA blends showed a new characteristic peak at 908 cm^{-1}, which corresponded to the characteristic peak of the formed sc-PLA crystals. Besides, with the increase of PDLA content, the intensity of characteristic peak at 908 cm^{-1} gradually increased, indicating that the content of sc-PLA crystal gradually increased. Meanwhile, the stretching vibration peak of C–CH$_3$ in PLPG matrix was 1036 cm^{-1}. As the addition of PDLA, such as PLPG/PDLA-20 blends, the characteristic peak shifted to the low frequency by 4 cm^{-1}. This is mainly because weak hydrogen bonds are formed between the PLLA in the sc-PLA crystal and the PDLA inter-segment CH$_2$–H···O=C groups in the PLPG/PDLA blends. Hydrogen bonding in the samples is of great interest due to the determination of the phase segregation.[36,37] As a result, the

stretching vibration peak of –C–CH$_3$ was blue-shifted. The results indicated that sc-PLA crystal was *in situ* formed by hydrogen bonding between PLLA segments and PDLA segments in the samples.

Non-isothermal crystallization behavior of PLLA segments in the blend of PLPG with PDLA

The thermal behavior of the samples was qualitatively studied by DSC. The results and the data were shown in Fig. 2(a) and Table 1. Clearly, the glass transition temperature (T_g) of the samples was about 54 °C, which implied no phase separation was occurred in the samples. The PLPG matrix showed a single melting peak (T_m) at 161.87 °C, which was attributed to PLLA segments in the PLPG copolymers. Meanwhile, the blends

Table 2 Non-isothermal crystallization parameters of the samples at a cooling rate of 2.5 °C min^{-1}

Samples	$T_c{}^a$ (°C)	ΔH_c (J g^{-1})	$X_c{}^b$ (%)
PLPG	—	—	—
PLPG/PDLA-5	120.19	29.02	31.20
PLPG/PDLA-10	123.69	25.59	27.51
PLPG/PDLA-15	124.76	20.97	22.55
PLPG/PDLA-20	123.13	17.12	18.41

^{a} T_c is the peak temperature of crystallization from the melt. ^{b} The values of X_c are estimated from $X_c = \Delta H_c/f\Delta H_m^\infty$, where $\Delta H_m^\infty = 93$ J g^{-1} and f is the weight fraction of PLLA in the samples.

Table 3 The overall crystallization kinetic parameters of the samples at 115 °C, 120 °C, 125 °C and 130 °C

| Samples	T_c (°C)	$t_{0.5}$ (min)	n	k (min^{-n})
PLPG/PDLA-5	115	2.33	2.42	6.17×10^{-2}
	120	2.58	2.30	1.90×10^{-1}
	125	2.98	2.02	3.19×10^{-1}
	130	4.13	2.13	2.04×10^{-1}
PLPG/PDLA-10	115	1.63	2.53	1.37×10^{-1}
	120	1.80	2.10	1.38×10^{-1}
	125	2.31	2.49	1.60×10^{-1}
	130	2.75	2.30	1.71×10^{-1}
PLPG/PDLA-15	115	1.36	2.53	5.03×10^{-2}
	120	1.65	2.01	7.38×10^{-2}
	125	1.85	2.21	1.50×10^{-1}
	130	2.76	2.29	1.46×10^{-1}
PLPG/PDLA-20	115	1.58	2.79	1.94×10^{-2}
	120	1.79	2.83	4.28×10^{-2}
	125	2.03	2.13	7.49×10^{-2}
	130	3.46	2.77	1.45×10^{-1}
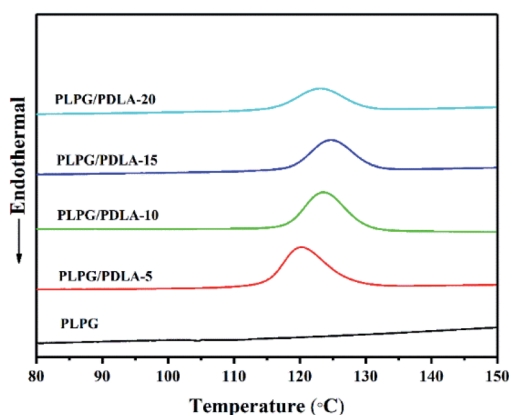
Fig. 3 Non-thermal crystallization curves of the samples at a cooling rate of 2.5 °C min^{-1}.
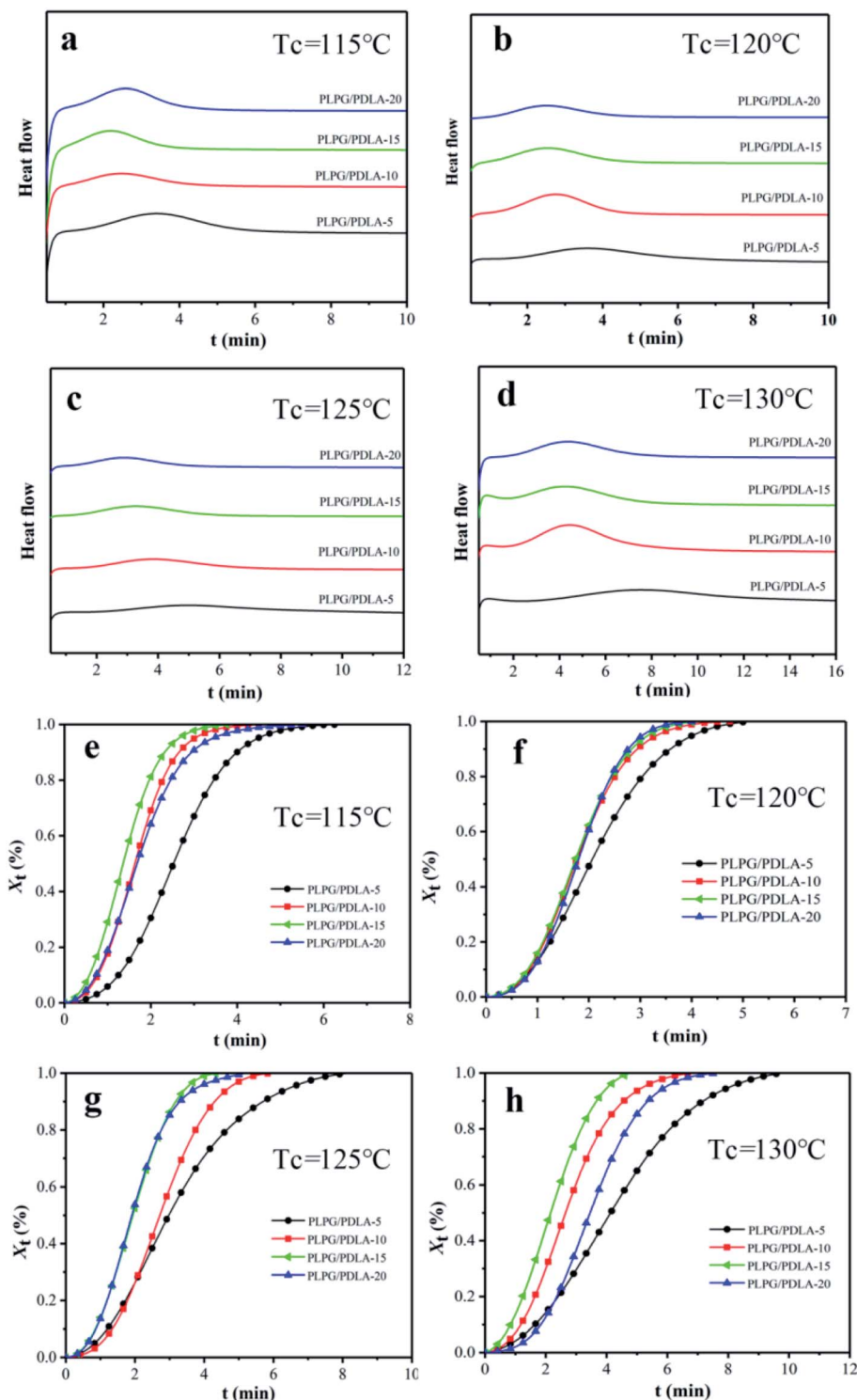
Fig. 4 DSC heat flow at T_c of 115 °C (a), 120 °C (b), 125 °C (c) and 130 °C (d), and X_t from DSC as a function of time for the samples crystallized at 115 °C (e), 120 °C (f), 125 °C (g) and 130 °C (h).

exhibited a higher T_m at 213 °C, which was due to the melt of sc-PLA crystals. This result indicated that sc-PLA crystals were formed by PLLA segments in the PLPG copolymer with PDLA segments. Interestingly, the melting endotherm of PLLA ($\Delta H_{m\text{-}hc}$) and sc-PLA ($\Delta H_{m\text{-}sc}$) in the samples was varied with the PDLA

content. With the increase of PDLA content, $\Delta H_{m\text{-}sc}$ increased from 7.57 to 26.19 J g^{-1}, and $\Delta H_{m\text{-}hc}$ decreased from 28.33 to 16.75 J g^{-1}. This is mainly because that the increased content of PDLA had resulted into a higher concentration of sc-PLA and a higher crystallinity of sc-PLA ($X_{c\text{-}sc}$), and therefore a lower

crystallinity of PLLA (X_{c-hc}) in the samples. These results proved that the change of the composition of the samples could be used to regulate the content of sc-PLA. Besides, the total crystallinity of the samples ($X_{c-hc+sc}$) increased with the increase of PDLA content. Meanwhile, with the increase of PDLA content, the peak temperature of cold crystallization of the samples decreased, which again confirmed the formation of sc-PLA between PDLA and PLLA segments within PLPG copolymers.

To further investigate the formation of sc-PLA crystals in the samples, WAXD was used to study the crystal structure of the samples, and the results were shown in Fig. 2(b). Obviously, the crystallization peaks of PLLA segments in the PLPG and the formed sc-PLA in the blends were clearly shown in WAXD spectra. The crystallization peaks at 15.0°, 16.9°, 19.2° and 22.5° were attributed to the α-form crystals of PLLA, which were corresponding to the (010), (200)/(110), (203) and (210) lattice planes, respectively.[38–40] Besides, three diffraction peaks at 11.9°, 20.9° and 24.0° could be assigned to (110), (300)/(030) and (220) planes of sc-PLA, respectively.[41] Importantly, the peak intensity of sc-PLA increased with the increase of PDLA content. These results indicated that sc-PLA was formed between the cocrystallization of PLLA segments in PLPG and PDLA, which was consistent with the results of DSC.

In order to examine the effect of PDLA on the crystallization kinetics of PLLA segments in the samples, the non-isothermal behavior were studied by DSC with a cooling rate of 2.5 °C min^{-1}. The results were depicted in Fig. 3 and the data were shown in Table 2. In general, a higher T_c under the cooling conditions indicates a faster crystallization rate.[42,43] Clearly, there were no crystallization peaks of PLLA segments in the PLPG copolymer, indicating that the crystallization of PLLA segments was difficult at 2.5 °C min^{-1}. Meanwhile, the broad crystallization peaks appeared in the DSC curves with the addition of PDLA. T_c of PLLA segments in the samples shifted to a higher temperature with PDLA up to 15 wt%, and decreased as the content of PDLA reached to 20 wt%. This is due to the nucleation effect of the sc-PLA and epitaxial crystallization of PLLA.[44] It can be concluded that the addition of PDLA significantly accelerated the crystallization ability of PLLA segments in the samples compared with that of PLPG. T_c of PLPG/PDLA-15 sharply increased to 124.76 °C with a significant higher X_c of 22.55%. However, further increase of PDLA content resulted into decreased T_c. This can be ascribed to the higher PDLA content that would impede the diffusion of PLLA segments. And the addition of PDLA accelerated the formation and crystallization of sc-PLA, thus resulting into a lower PLLA content in the samples. Moreover, the formed sc-PLA would act as physical crosslinking points, and have adverse impact on crystallization process. The results of the non-isothermal crystallization showed that the formed sc-PLA could accelerate the crystallization of PLLA segments in the samples.

Isothermal crystallization

In order to further study the accelerating effect of PDLA on the thermal properties of PLLA segments in the samples, the isothermal crystallization process was analyzed by DSC at 115,
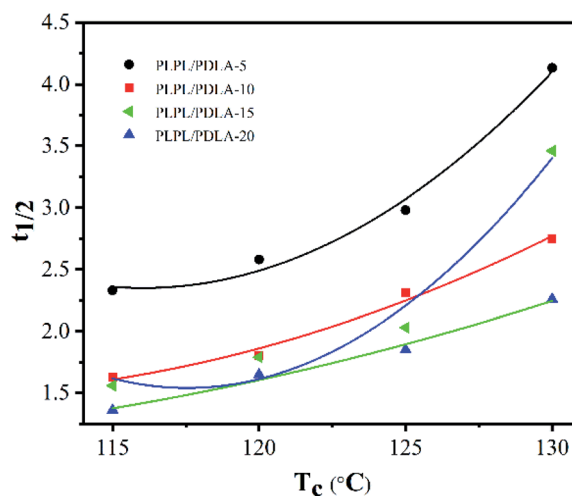

Fig. 5 $t_{0.5}$ of the samples at different T_c as the function of PDLA content.

120, 125 and 130 °C, respectively. The relative crystallinity (X_t) was calculated by the eqn (5).

$$X_t = \frac{\int_0^t \left(\dfrac{\mathrm{d}H}{\mathrm{d}t}\right)\mathrm{d}t}{\int_0^\infty \left(\dfrac{\mathrm{d}H}{\mathrm{d}t}\right)\mathrm{d}t} = \frac{\Delta H_t}{\Delta H_\infty} \tag{5}$$

where $\mathrm{d}H/\mathrm{d}t$ was the instantaneous rate of enthalpy change at time t, ΔH_t was defined as the heat enthalpy at time t, and ΔH_∞ was the total heat enthalpy.

The enhancement of PDLA on the crystallization ability of PLLA segments in the samples was studied, and the heat flow and X_t were shown in Fig. 4. As seen from Fig. 4(a)–(d), the exothermal peak was quite broad for the samples with the lower PDLA content at the selected T_c. Specially, with the increase of PDLA content, the exothermal peak gradually narrowed and X_t quickly increased, which implied the crystallization was accelerated of the effect of PDLA on PLLA segments in the samples. The improving influence of PDLA on PLLA segments in samples was further investigated and the results were shown in Fig. 4(e)–(h). Clearly, X_t of all the samples were typical S-shape curves, and the induction period could be found in the early stage. Meanwhile, there was an obvious increase in the conversion of crystallinity relative to the initial stage and X_t decreased as the content of PDLA further increased. This is because that the formed sc-PLA decreased the energy barrier or surface free energy barrier for PLLA nucleation. On the other hand, a higher PDLA content would lead to a higher content of sc-PLA, thus resulted in a higher X_{c-sc} and lower X_{c-hc} in the samples. Furthermore, the heterogeneous nucleation sites increased with the increase of PDLA content, thus the crystallization rate of PLLA segments in the samples was increased. Hence, addition of PDLA increased overall crystallization rate of PLLA segments in the samples.

The crystallization half-time ($t_{0.5}$), which is the time needed to accomplish half of the whole crystallinity, was calculated at $X_t = 50\%$. And the results were depicted in Fig. 5. As seen from
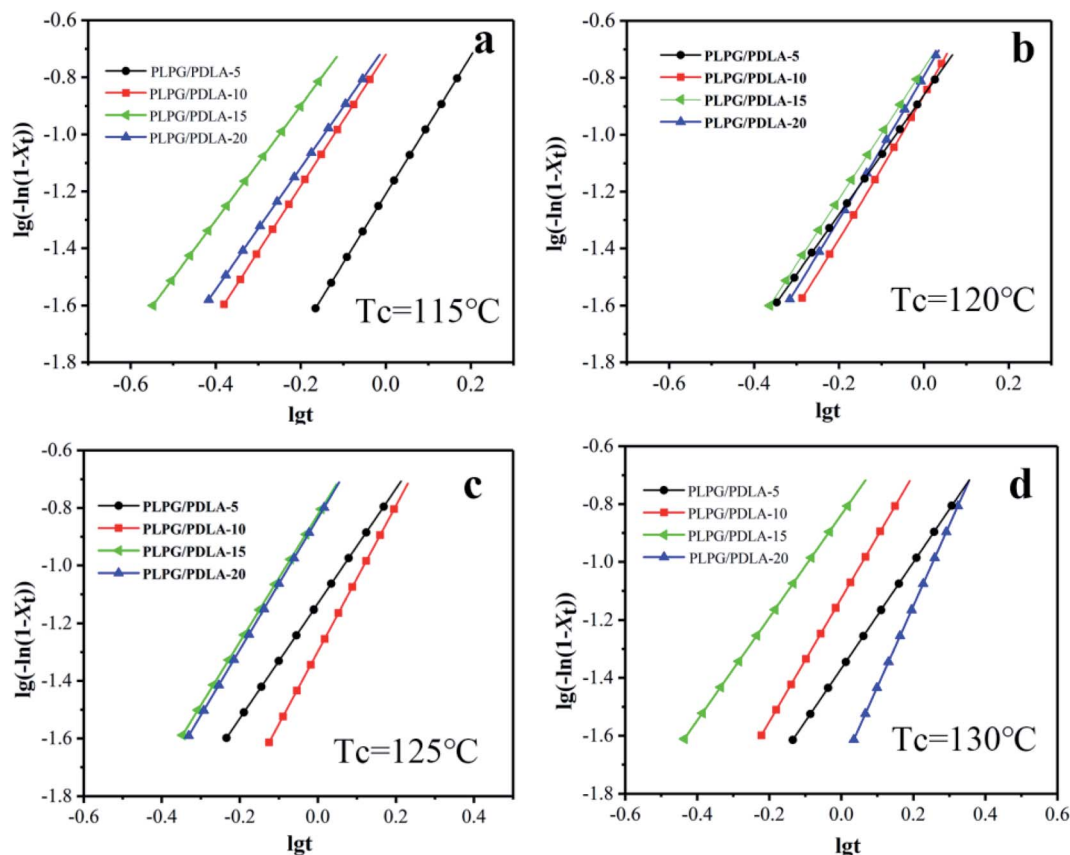
Fig. 6 Plots of log($-\ln(1 - X_t)$) versus log t of the isothermal crystallization at 115 °C (a), 120 °C (b), 125 °C (c) and 130 °C (d).

Fig. 5, with the addition of PDLA content, T_c decreased from 130 °C to 115 °C and $t_{0.5}$ gradually decreased as well. This can be ascribed to that the degree of subcooling lower, the higher mobility molecular chains would difficult to be fixed to the lattice orderly. For example, $t_{0.5}$ of PLPG/PDLA-15 decreased from 2.76 min to 1.36 min as T_c decreased from 130 °C to 115 °C. Moreover, with the increase of PDLA content, $t_{0.5}$ decreased under the same T_c. This is because that the more nucleating agents resulted into more nucleating sites. However, $t_{0.5}$ decreased as the content of PDLA increased to 20 wt%. This
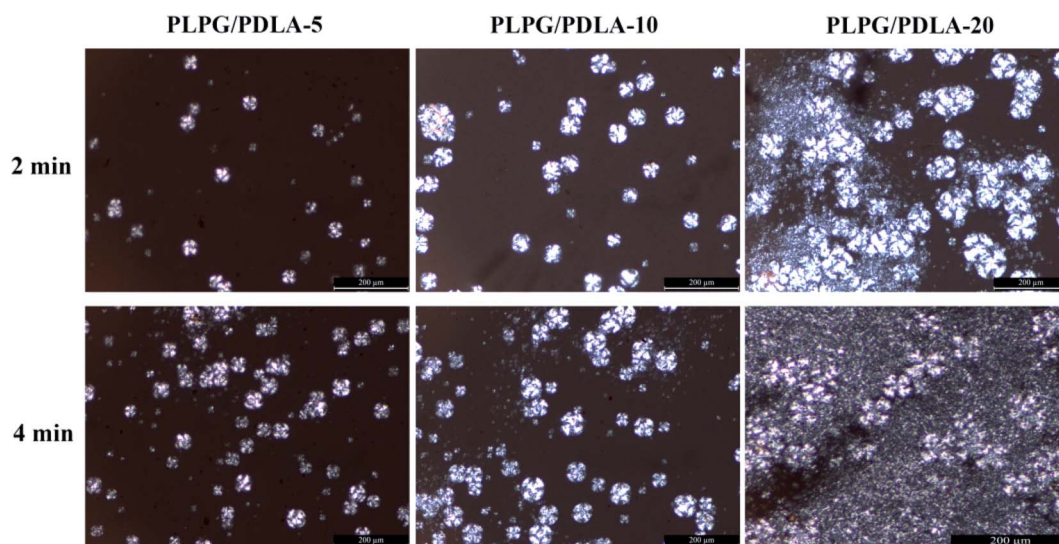

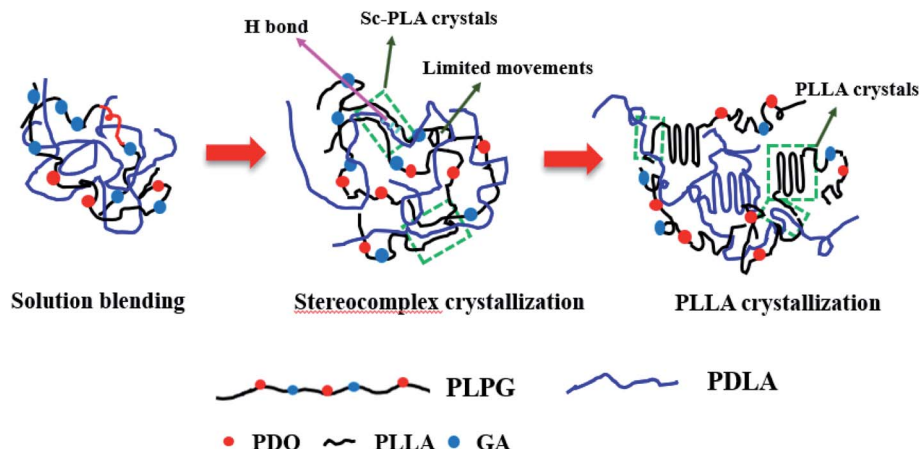Fig. 7 POM pictures of the samples at 125 °C for 2 min and 4 min.

Fig. 8 The nucleation mechanisms of PLPG using PDLA as nucleating agents.

is owing to that the crystallinity of sc-PLA crystal increases significantly with the increase of PDLA, which in turn reduced the crystallinity of PLLA segment in the samples. Indeed, as the content of PLDA reached to 10 or 15 wt%, $t_{0.5}$ of the samples at 120 °C and 125 °C decreased, and with the content of PDLA reached to 20 wt%, $t_{0.5}$ of the samples at 130 °C increased. These results implied that the introduction of PDLA would improve the crystallization ability of PLLA segments in the samples, which was in consistent with the results of non-isothermal crystallization behavior of the samples.

The Avrami eqn (6) was usually used to describe the isothermal crystallization process of polymers.[45]

$$\log[-\ln(1 - X_t)] = \log k + n\log t \qquad (6)$$

where n is the Avrami index that is related to the crystal growth mechanism and crystallite morphology. k is the overall crystallization rate constant. Specially, n and k can be acquired from the slope and intercept when $\log(-\ln(1 - X_t))$ *versus* $\log t$ was
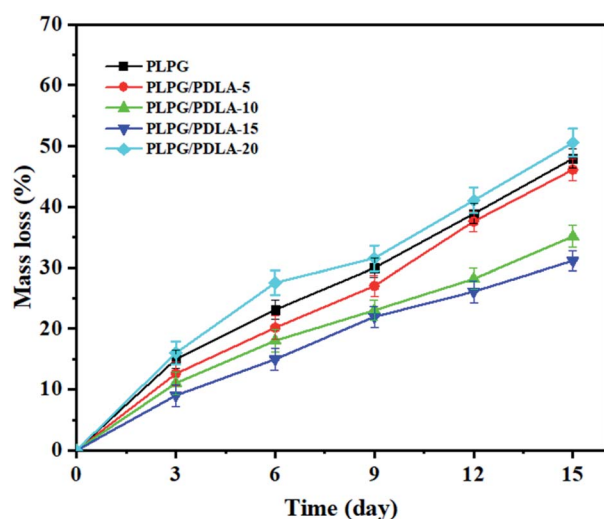
ploted by the Avrami eqn (6). Lorenzo *et al.* reported that X_t was chosen to evaluate n and k ranging from 3% to 20%. The fitted plots for the samples at the selected T_c were shown in Fig. 6 and the data were exhibited in Table 3. The overall crystallization kinetics of PLLA segments in the samples of the primary crystallization range can be described very well by the Avrami equation. Meanwhile, the values of n for all the samples varied between 2.0 and 3.0 as shown in Table 3. This result indicated that the crystal growth was a heterogeneously nucleated three dimensional spherulites growth mechanism.

Spherulite morphology during isothermal crystallization

The crystallization promoting effect of nucleating agents mainly relies on the improvement on nucleation. To further reveal the nucleation enhancement of the formed sc-PLA on PLLA segments in the samples, the growing spherulite morphologies of the samples were analyzed by POM during T_c at 125 °C for 2 min and 4 min, respectively, and the results were depicted in Fig. 7. Clearly, with the introduction of PDLA, a small number of spherulites appeared at the initial stage of crystallization of 2 min. Meanwhile, as the isothermal time reached to 4 min, much more spherulites were emerged. And compared with other content of PDLA, PLPG/PDLA-20 samples possessed more and more spherulites with superposition phenomenon. These results indicated that the formed sc-PLA had evidently nucleation ability for the samples and the addition of PDLA could greatly improve the crystallization ability of PLLA segments in the samples.

Fig. 9 The weight loss of the samples during enzymatic degradation for 14 days.

Nucleation mechanisms

In general, chemical nucleation and epitaxial nucleation mechanisms are used to describe the roles of nucleating agents. The nucleation mechanisms of PLPG matrix using PDLA as nucleating agents were shown in Fig. 8. Since there was no chemical reaction between PDLA and PLLA, so the nucleation mechanism of sc-PLA was not chemical nucleation mechanism. Sc-PLA crystals were formed by hydrogen bond between PDLA
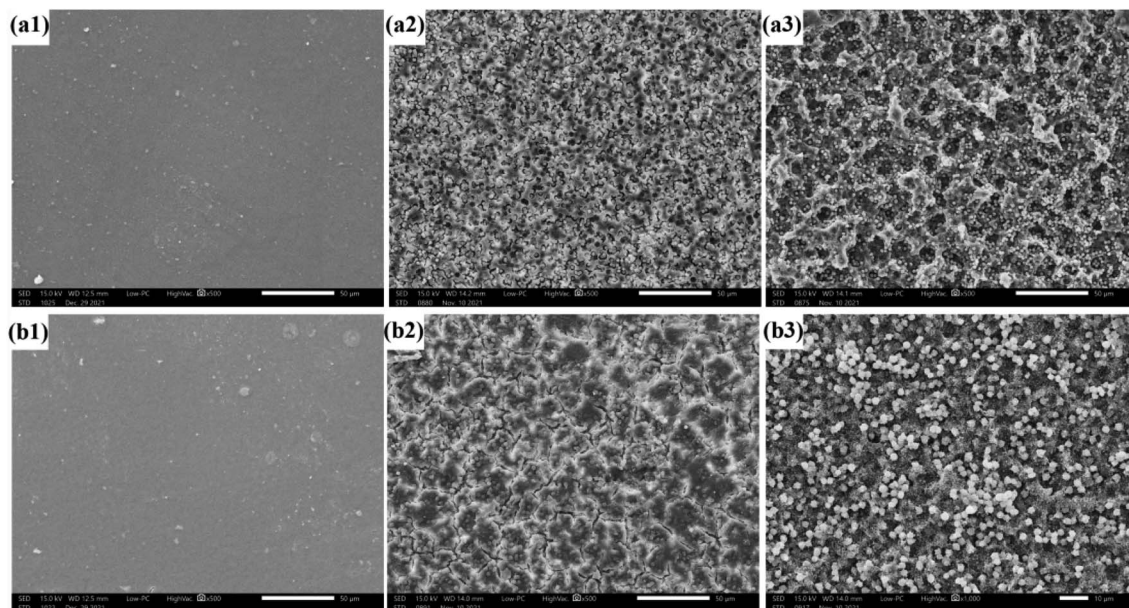
Fig. 10 The surface morphology of PLPG/PDLA-10 and PLPG/PDLA-15 during enzymatic degradation for 14 days ((a_1 and b_1) 0 day, (a_2 and b_2) 8 days, (a_3 and b_3) 14 days).
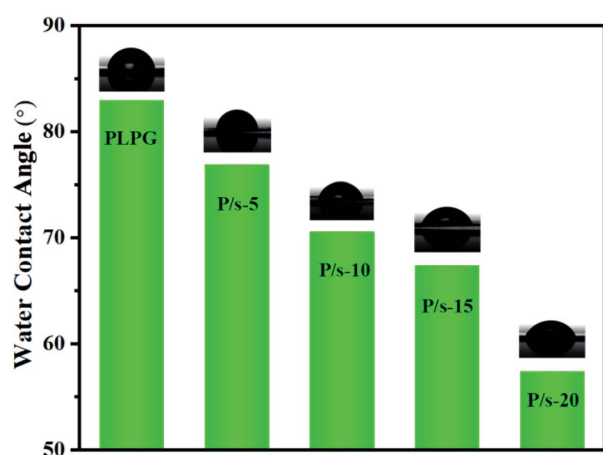

Fig. 11 Water contact angle of the samples.

and PLLA segments in the samples, which was a type of physical force rather than chemical bond.

Lotz and Wittmann reported that epitaxial crystallization of the helical polymers could be used to describe the crystallization of PE, iPP and others.[46] The basic requirement for epitaxial nucleation is that the polymer matrix matches with the two-dimensional lattice of nucleating agents. Generally, the acceptable scope of a lattice match needs to be more than 85%. Without doubt, the similarity or lattice match between nucleating agents and polymers is important in epitaxially nucleating. Because the crystal structure of the formed sc-PLA was the same as that of PLPG matrix, sc-PLA would accelerate the crystallization of the second crystalline phase by decreasing the activation free energy. In the above experiments, the samples were isothermally treated at 155 °C to complete the crystallization of sc-PLA. WAXD results demonstrated that the sc-PLA

formed with no homo-crystallites at 155 °C. Therefore, the epitaxial nucleation of PLPG matrix would occur during the followed isothermal crystallization process.

Enzymatic degradation properties

As shown in Fig. 9, W increased linearly with the increase of degradation time till 2 weeks. PLPG matrix presented the fastest degradation rate of 50.56%. With the increase of PDLA, W gradually decreased. W of PLPG/PDLA-15 and PLPG/PDLA-20 was evidently lower than those of the other samples, which were 35.12% and 31.13%, respectively. It is believed that proteinase K can only degrade the amorphous regions of PLLA. With the increase of PDLA content, more sc-PLA was formed due to the increased heterogeneous nucleation sites. The formed sc-PLA improved the crystallization ability of PLLA segments in the samples, thus leading to a higher degree of crystallization. Furthermore, the formed sc-PLA was more difficult to degrade by proteinase K as compared with PLLA.

In general, polymer degradation by proteinase K is surface erosion degradation, the surface morphology changes of PLPG/PDLA-10 and PLPG/PDLA-15 during the enzymatic degradation for 14 days were observed by SEM, and the images were shown in Fig. 10(a1)–(a3) and (b1)–(b3). The surface of the undegraded samples was relatively smooth and has some irregular spherulites on the surface. After 8 days of protease K degradation, the amorphous region on the surface of PLPG/PDLA-10 was eroded by protease K. Besides, the surface became rough with a small number of pits, and spherulites can be observed in the pits. This is because the amorphous area around the spherulites could be eroded by proteinase K but not the spherulites. As the degradation time reached to 14 days, the amorphous area of the samples was further reduced and much more granular structure appeared on the surface of the samples. Compared to PLPG/
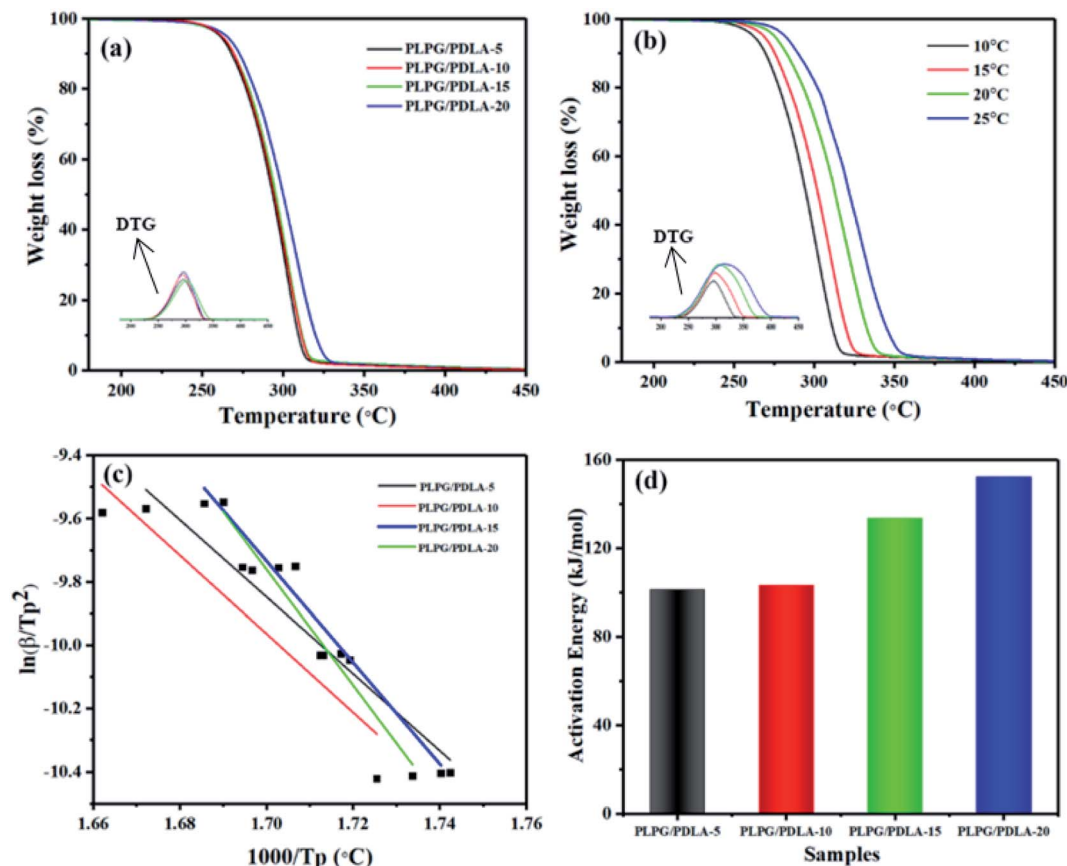
Fig. 12 TGA and DTG curves of the samples at 10 °C min^{-1} (a), TGA and DTG curves of the PLPG/PDLA-10 at 10, 15, 20 and 25 °C min^{-1} (b), Kissinger method used to the experimental data of the samples (c), apparent E_a data (d).

PDLA-10, PLPG/PDLA-15 showed relatively smaller amount of pits and amorphous regions on the surface after both 8 and 14 days degradation, the SEM results were in consistent with the mass loss rate in the enzymatic degradation study.

Hydrophilic and hydrophobic properties

Generally, the hydrophilicity and hydrophobicity of the material surface are related to the surface roughness. The increase in the roughness of the material surface would increase the contact area between the water droplet and the material surface. Fig. 11 was the water contact angle of the samples measured by static contact angle. As seen, the water contact angle of PLPG matrix was 82.9°. Meanwhile, with the increase of the amount of PDLA, the water contact angle of the samples gradually decreased. For example, the water contact angle of PLPG/PDLA-5 was 76.8°, and when the PDLA content increased to 20 wt%, the water contact angle of PLPG/PDLA-20 decreased to 57.3°. The reason for this result was the introduction of PDLA generated sc-PLA crystals on the surface in the samples, resulting in a rougher surface of the samples.

Thermal degradation behavior

TGA is commonly used to quantitative analyze the mass loss and apparent activation energy of polymers. The effect of PDLA on the thermal stability of the samples was also studied by TGA

at a temperature ramping rate of 10 °C min^{-1}, and the results were shown in Fig. 12. As seen from Fig. 12(a), the samples were quite stable from 30 °C to 230 °C, and a single-stage thermal degradation weight loss process was observed with the further increase of the temperature to 450 °C. Besides, with the increase of PDLA content, the thermal stability of the samples was increased. The PLPG/PDLA-20 possessed the highest thermal stability with the temperature at maximum mass loss rate (T_P) at about 306.56 °C, and was almost 10 °C higher than that of the PLPG matrix, indicating that the formed sc-PLA increased thermal stability of the samples. Furthermore, the formed sc-PLA would be acted as nucleation agents which accelerated the crystallization rate of PLLA segments in the samples, thus resulted into more PLLA crystals.

Moreover, the kinetic of thermal degradation of the samples was researched using the Kissinger method. The heating rate was selected as 10, 15, 20 and 25 °C min^{-1}, and the results were presented in Fig. 12(b). As seen, the TGA and DTG plots shifted to the higher temperature region with the increase of heating rate. This can be ascribed to the shorter time to reach a specific temperature and the faster release of gaseous products.

It is well known that the Kissinger method commonly uses the inflection point temperatures as the basis for study the kinetics of thermal degradation, and the values were calculated using eqn (7).[47]
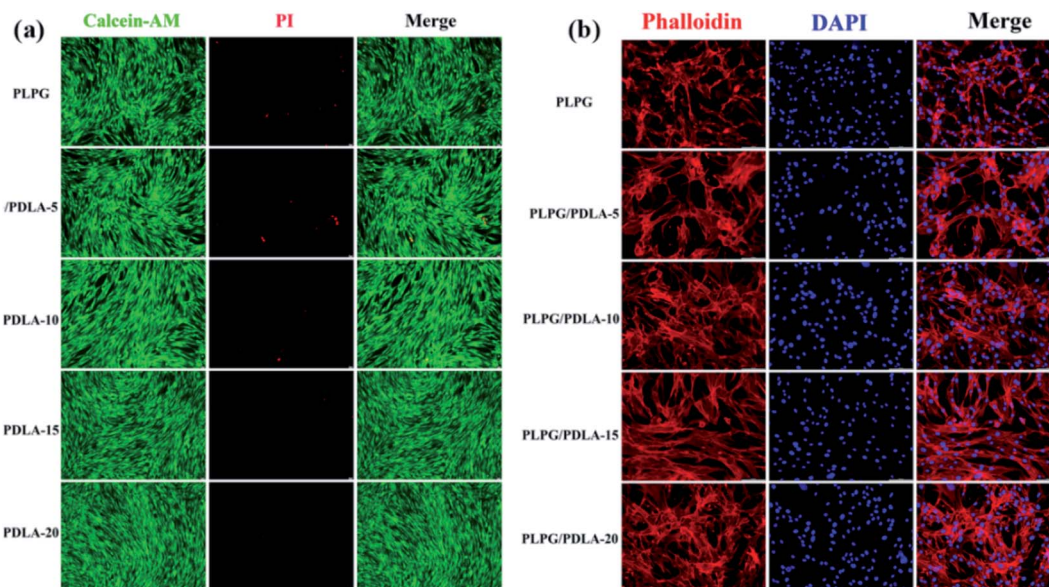
Fig. 13 The live/dead cell viability (a) and the representative immunofluorescence microscopy images (b) of hADSCs cultured with the extracts of the samples for 48 h (scale bar = 50 μm).

$$\ln\frac{\beta}{T_P{}^2} = \frac{E_a}{R} \times \frac{1}{T_P} + \ln\frac{AR}{E} \qquad (7)$$

where β is defined as the heating rate. A is the pre-exponential factor. R is the gas constant.

The data and the graph of $\ln\frac{\beta}{T_P{}^2}$ *versus* $-1000/T_P$ of the samples were shown in Fig. 12(c) and (d). As seen from Fig. 12(c), the smooth linear fitted lines confirmed that
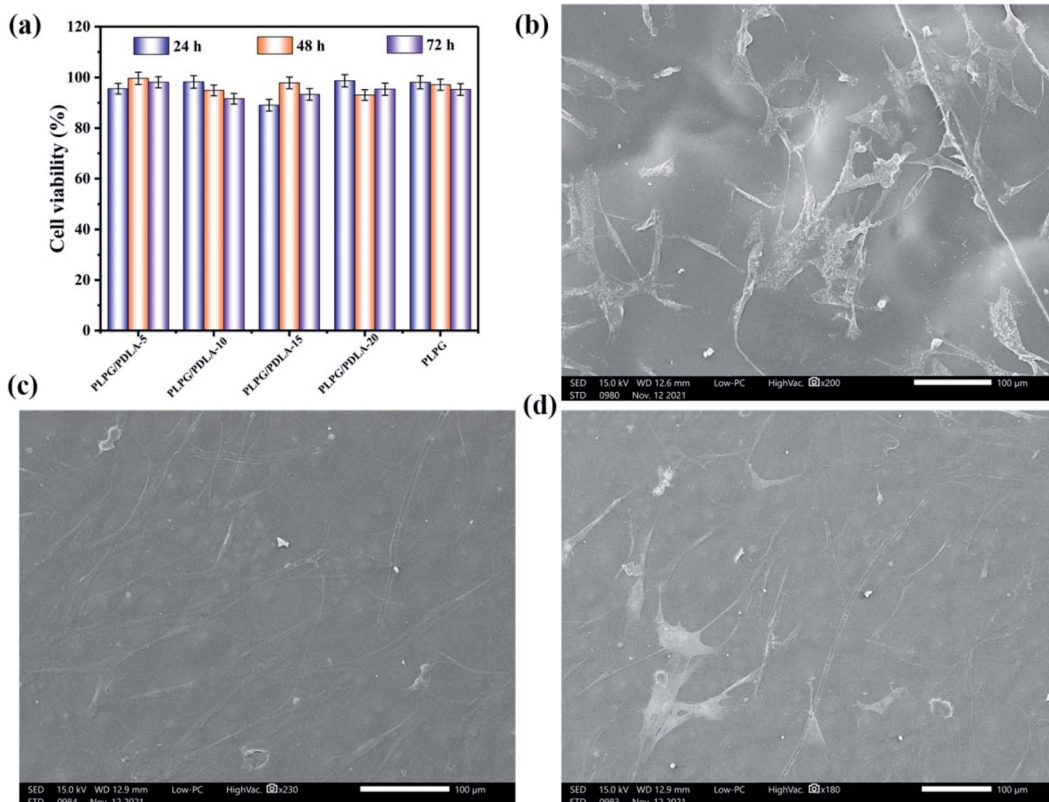

Fig. 14 CCK-8 assay of hADSCs cultured with the samples for 24, 48 and 72 h (a), and SEM images of hADSCs grown on the surface of the PLPG (b), PLPG/PDLA-10 (c) and PLPG/PDLA-15 (d).

Kissinger method can describe the thermal decomposition kinetics of the samples very well. Besides, the average E_a of the samples can be calculated by Kissinger method from Fig. 12(d). With the increase of PDLA content, E_a of the samples was increased. This is because that the formed sc-PLA crystals possessed higher thermal stability than that of PLLA. On the other hand, the formed sc-PLA crystals acted as nucleating agents, and promoted the crystal formation of PLLA, thus resulting to higher content of PLLA crystals in the samples. For example, E_a of the PLPG/PDLA-5 was 101.1 kJ mol^{-1}, and as the content of PDLA increased to 20 wt%, E_a increased to 152.2 kJ mol^{-1}. These results implied that the formed sc-PLA crystals contributed greatly to E_a of the samples.

In vitro cytotoxicity study

The cytotoxicity of the samples was studied by a cell culture method and evaluated using CCK-8 and live/dead staining. The results of cell viability of hADSCs cultured with the extracts of the samples for 48 h was shown in Fig. 13(a). Generally, the live cells stained with calcein-AM solution were green fluorescence, and the dead cells stained with PI solution were red fluorescence. Clearly, all the samples showed very low cytotoxicity as very few dead cells were observed after 48 hour culture. Meanwhile, the morphology of hADSCs after culturing was studied using cytoskeleton and the nucleus staining methods, which used RBITC-labeled phalloidin (red color) and dapi (blue color). The hADSCs that cocultured with the extracts of the samples showed a well-spread shape with long, thin filopodia, a well-organized pattern of numerous and straight actin stress fibers were observed as well (Fig. 13(b)). All these results indicated that the PLPG/PDLA blends possessed the very low cytotoxicity.

Furthermore, the cytotoxicity of hADSCs cocultured with the samples was further tested by CCK-8 assay, and the results were shown in Fig. 14(a). As shown, the cell viabilities of all the samples were all above 80%, and when the cultured time increased to 72 h, the cell viabilities also increased. The results again confirmed that all the samples have very low cytotoxicity. Fig. 14(b)–(d) showed that the hADSCs adhered very well on the samples on day 7, respectively, showing a spindle-shaped and well spread cell morphology. Furthermore, hADSCs spread and formed cell layers, on the surfaces of the samples. These results suggested that the PLPG/PDLA blends have the potential to be used in biomedical applications.

Conclusion

PDLA exhibited the significant accelerating effect on the crystallization ability of PLLA segments in the samples. The results of non-isothermal crystallization and WAXD proved that sc-PLA crystals were formed by H bond between PLLA segments in PLPG matrix and PDLA. ΔH_m of both PLLA and sc-PLA in the samples increased with the increase of PDLA content. Besides, no crystallization peak of PLPG matrix was detected in the non-isothermal crystallization, and with the addition of PDLA, T_c of the samples shifted to higher temperature. Moreover, $t_{0.5}$ decreased from 4.13 min to 2.33 min at 110 °C as the content of

PDLA increased from 5 wt% to 20 wt%. Importantly, the enhancement of crystallization ability was more prominent with the increase of PDLA content. POM results indicated that with the increase of PDLA content, the crystallization behavior of the samples was significantly improved due to the enhancement of the nucleation density. The results of enzymatic degradation showed that with addition of PDLA, the mass loss of the samples gradually decreased. TGA results showed that the apparent activation energy of thermal degradation was also affected by the addition of PDLA. The values of E_a of the samples increased from 101.1 to 152.2 kJ mol^{-1}. Furthermore, the results of cytotoxicity study of the blends indicated that the samples possessed good cytocompatibility and are good candidates for biomedical applications.

Conflicts of interest

There are no conflicts to declare.

Acknowledgements

References

1 X. Shi, J. Qin, L. Wang, L. Ren, F. Rong, D. Li, R. Wang and G. Zhang, Introduction of stereocomplex crystallites of PLA for the solid and microcellular poly(lactide)/poly(butylene adipate-*co*-terephthalate) blends, *RSC Adv.*, 2018, **8**, 11850–11861.

2 B. Zhang, X. Bian, D. Zhou, L. Feng, G. Li and X. Chen, Toughening modification of PLLA by combination of copolymerization and *in situ* reactive blending, *RSC Adv.*, 2016, **6**, 113366–113376.

3 W. Li, X. Chen, Y. Ma and Z. Fan, The accelerating effect of the star-shaped poly(D-lactide)-*block*-poly(L-lactide) stereoblock copolymer on PLLA melt crystallization, *CrystEngComm*, 2016, **18**, 1242–1250.

4 M. Hozhabr, P. Dong, K. Ren, X. Han and L. Gu, Micromechanical analysis of bioresorbable PLLA/Mg composites coated with MgO: Effects of particle weight fraction, particle/matrix interface bonding strength and interphase, *Composites, Part B*, 2019, **162**, 129–133.

5 J. Li, Q. Chen, Q. Zhang, T. Fan, L. Gong, W. Ye, Z. Fan and L. Cao, Improving Mechanical Properties and Biocompatibilies by Highly Oriented Long Chain Branching Poly(lactic acid) with Bionic Surface Structures, *ACS Appl. Mater. Interfaces*, 2020, **12**, 14365–14375.

6 P. Chou, M. Mariatti, A. Zulkifli and S. Sreekantan, Evaluation of the flexural properties and bioactivity of bioresorbable PLLA/PBSL/CNT and PLLA/PBSL/TiO$_2$ nanocomposites, *Composites, Part B*, 2012, **43**, 1374–1384.

7 Y. Zheng, J. Zhou, F. Du, Y. Bao, G. Shan, L. Zhang, H. Dong and P. Pan, Formation of Mesomorphic Polymorph, Thermal-Induced Phase Transition, and Crystalline Structure-Dependent Degradable and Mechanical

Properties of Poly(p-dioxanone), *Cryst. Growth Des.*, 2019, **19**, 166–176.

8 X. Xu, Q. Li and C. Xiong, Crystallization behavior of poly(p-dioxanone) with cyclodextrin complex and nucleation mechanism discussion, *RSC Adv.*, 2016, **6**, 87169–87178.

9 F. Zhao, J. Sun, W. Xue, F. Wang, M. King, C. Yu, Y. Jiao, K. Sun and L. Wang, Development of a polycaprolactone/poly(p-dioxanone) bioresorbable stent with mechanically self-reinforced structure for congenital heart disease treatment, *Bioact. Mater.*, 2021, **6**, 2969–2982.

10 Y. Qu, K. Lu, Y. Zheng, C. Huang, G. Wang, Y. Zhang and Q. Yu, Photothermal scaffolds/surfaces for regulation of cell behaviors, *Bioact. Mater.*, 2022, **8**, 449–477.

11 D. Cao, X. Chen, F. Cao, W. Guo, J. Tang, C. Cai, S. Cui, X. Yang, L. Yu and J. Ding, An Intelligent Transdermal Formulation of ALA-Loaded Copolymer Thermogel with Spontaneous Asymmetry by Using Temperature-Induced Sol-Gel Transition and Gel-Sol (Suspension) Transition on Different Sides, *Adv. Funct. Mater.*, 2021, **31**, 2100349.

12 Y. Chen, Z. Li, P. Pan, R. Zeng and X. Zhang, Tumor-Specific ONOO-Nanogenerator for Improved Drug Delivery and Enhanced Chemotherapy of Tumor, *ACS Nano*, 2021, **15**, 11514–11525.

13 S. Cui, Y. Wei, Q. Bian, Y. Zhu, X. Chen, Y. Zhuang, M. Cai, J. Tang, L. Yu and J. Ding, Injectable Thermogel Generated by the "Block Blend" Strategy as a Biomaterial for Endoscopic Submucosal Dissection, *ACS Appl. Mater. Interfaces*, 2021, **13**, 19778–19792.

14 C. Chen, L. Chen, L. Cao, L. Yu and J. Ding, Effects of L-lactide and D,L-lactide in poly(lactide-*co*-glycolide)-poly(ethylene glycol)-poly(lactide-*co*-glycolide) on the bulk states of triblock copolymers, and their thermogellation and biodegradation in water, *RSC Adv.*, 2014, **4**, 8789–8798.

15 P. Purnama, M. Samsuri and I. Iswaldi, Properties Enhancement of High Molecular Weight Polylactide Using Stereocomplex Polylactide as a Nucleating Agent, *Polymers*, 2021, **13**, 1725.

16 G. Tao, Z. Zheng, L. Li, R. Bao, Z. Liu, B. Xie, M. Yang and W. Yang, Tailoring Crystalline Morphology by High-Efficiency Nucleating Fiber: Toward High-Performance Poly(L-lactide) Biocomposites, *ACS Appl. Mater. Interfaces*, 2018, **10**, 20044–20054.

17 H. Zhao, Y. Bian, M. Xu, C. Han, Y. Li, Q. Dong and L. Dong, Enhancing the crystallization of poly(l-lactide) using a montmorillonitic substrate favoring nucleation, *CrystEngComm*, 2014, **16**, 3896–3905.

18 A. Pei, Q. Zhou and L. Berglund, Functionalized cellulose nanocrystals as biobased nucleation agents in poly (l-lactide)(PLLA)-Crystallization and mechanical property effects, *Compos. Sci. Technol.*, 2010, **70**, 815–821.

19 T. Mathew, R. A. Sree, S. Aishwarya, K. Kounaina, A. G. Patil, P. Satapathy, S. P. Hudeda, S. S. More, K. Muthucheliyan, T. N. Kumar, A. V. Raghu, K. R. Reddy and Z. Farhan, Graphene-based functional nanomaterials for biomedical and bioanalysis applications, *FlatChem*, 2020, **23**, 100184.

20 K. T. Kim, T. D. Dao, H. M. Jeong, R. V. Anjanapura and M. A. Aminabhavi, Graphene coated with alumina and its

utilization as a thermal conductivity enhancer for alumina sphere/thermoplastic polyurethane composite, *Mater. Chem. Phys.*, 2015, **153**, 291–300.

21 D. P. Suhas, T. M. Aminabhavi, H. M. Jeong and A. V. Raghu, Hydrogen peroxide treated graphene as an effective nanosheet filler for separation application, *RSC Adv.*, 2015, **5**(122), 100984–100995.

22 S. Kumar, K. R. Reddy, C. V. Reddy, N. P. Shetti, V. Sadhu, M. V. Shankar, V. G. Reddy, A. V. Raghu and M. A. Aminabhavi, Metal Nitrides and Graphitic Carbon Nitrides as Novel Photocatalysts for Hydrogen Production and Environmental Remediation, *Nanostructured Materials for Environmental Applications*, 2015, vol. 153, pp. 291–300.

23 K. T. Kim, T. D. Dao, H. M. Jeong, R. V. Anjanapura and T. M. Aminabhavi, Graphene coated with alumina and its utilization as a thermal conductivity enhancer for alumina sphere/thermoplastic polyurethane composite, *Mater. Chem. Phys.*, 2015, **153**, 291–300.

24 K. Samira, G. Ismaeil and A. Foroud, A study on the crystallization kinetics of PLLA in the presence of Graphene Oxide and PEG-grafted-Graphene Oxide: Effects on the nucleation and chain mobility, *Composites, Part B*, 2019, **158**, 302–310.

25 B. Ma, H. Zhang, K. Wang, H. Xu, Y. He and X. Wang, Influence of scPLA microsphere on the crystallization behavior of PLLA/PDLA composites, *Compos. Commun.*, 2020, **21**, 100380.

26 J. Hu, J. Wang, M. Wang, Y. Ozaki, H. Sato and J. Zhang, Investigation of crystallization behavior of asymmetric PLLA/PDLA blend using Raman Imaging measurement, *Polymer*, 2020, **172**, 1–6.

27 H. Yin, X. Wei, R. Bao, Q. Dong, Z. Liu, W. Yang, B. Xie and M. Yang, Enantiomeric poly (d-lactide) with a higher melting point served as a significant nucleating agent for poly (l-lactide), *CrystEngComm*, 2015, **17**, 4334–4342.

28 L. Aliotta, P. Cinelli, M. Coltelli, M. Righetti, M. Gazzano and A. Lazzeri, Effect of nucleating agents on crystallinity and properties of poly (lactic acid)(PLA), *Eur. Polym. J.*, 2017, **93**, 822–832.

29 T. Fan, J. Qin, S. Lin, W. Ye, J. Li, Q. Zhang, L. Gong, D. Liu and Z. Fan, Enhancement of the crystallization and biocompatibility of poly (TMC-b-(LLA-ran-GA)) by poly (lactide) stereocomplex, *CrystEngComm*, 2019, **21**, 6269–6280.

30 T. Fan, J. Qin, S. Lin, W. Ye, Q. Liu, Z. Fan and Y. Wang, Enhancing crystallization behavior for optimized performances of poly(TMC-*b*-(LLA-*ran*-GA)) by PDLA/PLLA stereocomplex crystallization, *Polym. Adv. Technol.*, 2020, **31**, 1675–1687.

31 Y. Li, S. Xin, Y. Bian, Q. Dong, C. Han, K. Xu and L. Dong, Stereocomplex crystallite network in poly(D,L-lactide): formation, structure and the effect on shape memory behaviors and enzymatic hydrolysis of poly(D,L-lactide), *RSC Adv.*, 2015, **5**, 24352–24362.

32 H. Tsuji, S. Hyou and Y. Ikada, Stereocomplex formation between enantiomeric poly(lactic acid) s. 3. Calorimetric

studies on blend films cast from dilute solution, *Macromolecules*, 1991, **24**(20), 5651–5656.

33 X. Su, L. Feng and D. Yu, Formation of stereocomplex crystal and its effect on the morphology and property of PDLA/PLLA blends, *Polymers*, 2020, **12**, 2515.

34 H. Lu, S. Kazarian and H. Sato, Simultaneous Visualization of Phase Separation and Crystallization in PHB/PLLA Blends with *In Situ* ATR-FTIR Spectroscopic Imaging, *Macromolecules*, 2020, **53**, 9074–9085.

35 W. Li, X. Wu, X. Chen and Z. Fan, The origin of memory effect in stereocomplex poly (lactic acid) crystallization from melt state, *Eur. Polym. J.*, 2017, **89**, 241–248.

36 A. V. Raghu, G. S. Gadaginamath, N. Mathew, S. B. Halligudi and T. M. Aminabhavi, Synthesis, Characterization, and Acoustic Properties of New Soluble Polyurethanes Based on2,20-[1,4-Phenylenebis(nitrilomethylylidene)diphenol and 2,20-[4,40-Methylene-di-2-methylphenylene-1,10-bis(nitrilomethylylidene)]diphenol, *J. Appl. Polym. Sci.*, 2007, **106**, 299–308.

37 A. V. Raghu and H. M. Geong, Synthesis, characterization of novel dihydrazide containing polyurethanes based on N1,N2-bis[[4-hydroxyphenyl)methylene]ethanedihydrazide and various diisocyanates, *J. Appl. Polym. Sci.*, 2008, **107**(5), 3401–3407.

38 T. Fan, W. Ye, B. Du, Q. Zhang, G. Li, S. Lin, Z. Fan and Q. Liu, Effect of segment structures on the hydrolytic degradation behaviors of totally degradable poly(L-lactic acid)-based copolymers, *J. Appl. Polym. Sci.*, 2019, 47887.

39 H. Park and C. Hong, Relationship between the stereocomplex crystallization behavior and mechanical properties of PLLA/PDLA blends, *Polymers*, 2021, **13**, 1851.

40 L. Jiang, P. Lv, P. Ma, H. Bai, W. Dong and M. Chen, Stereocomplexation kinetics of enantiomeric poly(L-lactide)/poly(D-lactide) blends seeded by nanocrystalline cellulose, *RSC Adv.*, 2015, **5**, 71115–71119.

41 A. Gupta, A. Prasad, N. Mulchandani, M. Shah, M. R. Sankar, S. Kumar and V. Katiyar, Multifunctional Nanohydroxyapatite-Promoted Toughened High-Molecular-Weight Stereocomplex Poly(lactic acid)-Based Bionanocomposite for Both 3D-Printed Orthopedic Implants and High-Temperature Engineering Applications, *ACS Omega*, 2017, **2**, 4039–4052.

42 A. V. Raghu, G. S. Gadaginamath, S. S. Jawalkar, S. B. Halligudi and T. M. Aminabhavi, Synthesis, characterization, and molecular modeling studies of novel polyurethanes based on 2,2′-[ethane-1,2-diylbis(nitrilomethylylidene)]diphenol and 2,2′-[hexane-1,6-diylbis(nitrilomethylylidene)] diphenol hard segments, *J. Polym. Sci., Part A: Polym. Chem.*, 2006, **44**(20), 6032–6046.

43 A. V. Raghu, G. S. Gadaginamath, N. T. Mathew, S. B. Halligudi and T. M. Aminabhavi, Synthesis and characterization of novel polyurethanes based on 4,4′-[1,4-phenylenedi-diazene-2,1-diyl]bis(2-carboxyphenol) and 4,4′-[1,4-phenylenedi-diazene-2,1-diyl]bis(2-chlorophenol) hard segments, *React. Funct. Polym.*, 2007, **67**(6), 503–514.

44 K. Anderson and M. Hillmyer, Melt preparation and nucleation efficiency of polylactide stereocomplex crystallites, *Polymer*, 2006, **47**, 2030–2035.

45 H. Lu, R. Ma, R. Chang and Y. Tian, Evaluation of starch retrogradation by infrared spectroscopy, *Food Hydrocolloids*, 2021, **120**, 106975.

46 Y. Takenaka, H. Miyaji, A. Hoshino, A. Tracz, J. Jeszka and I. Kucinska, Interface structure of epitaxial polyethylene crystal grown on HOPG and MoS_2 substrates, *Macromolecules*, 2004, **37**, 9667–9669.

47 D. Monika and V. Katiyar, Thermal degradation kinetics of polylactic acid/acid fabricated cellulose nanocrystal based bionanocomposites, *Int. J. Biol. Macromol.*, 2017, **104**, 827–836.